Journal Pre-proofs

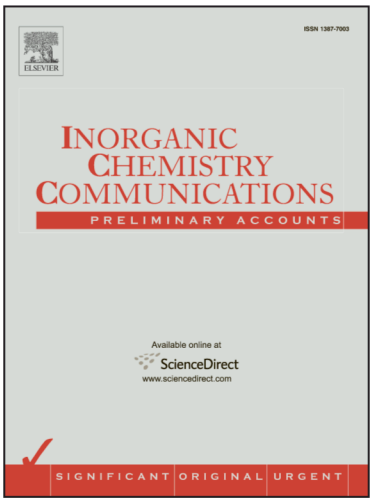

A novel "turn-off" fluorescent sensor for Al^{3+} detection based on quinoline-carboxamide-coumarin

Zichun Zhou, Wenjie Niu, Zhangqi Lin, Yanhong Cui, Xue Tang, Yujin Li

PII: S1387-7003(20)30758-9
DOI: https://doi.org/10.1016/j.inoche.2020.108168
Reference: INOCHE 108168

To appear in: *Inorganic Chemistry Communications*

Received Date: 17 March 2020
Revised Date: 1 August 2020
Accepted Date: 5 August 2020

Please cite this article as: Z. Zhou, W. Niu, Z. Lin, Y. Cui, X. Tang, Y. Li, A novel "turn-off" fluorescent sensor for Al^{3+} detection based on quinolinecarboxamide-coumarin, *Inorganic Chemistry Communications* (2020), doi: https://doi.org/10.1016/j.inoche.2020.108168

A novel "turn-off" fluorescent sensor for Al^{3+} detection based on quinolinecarboxamide-coumarin

Zichun Zhou, Wenjie Niu, Zhangqi Lin, Yanhong Cui, Xue Tang, Yujin Li*

College of Chemical Engineering, Zhejiang University of Technology, Hangzhou 310014, People's Republic of China.

Abstract:

Quinolinecarboxamides based on coumarin derivatives were efficiently synthesized and the optical properties were investigated. Compound **ZXQ** substituted by the diethylamino group on 7-position of coumarin exhibited blue fluorescence (λ_{em} ≈ 470 nm) with a high fluorescence quantum yield of 0.92 in Toluene and showed "turn-off" fluorescence property for Al^{3+}. Probe **ZXQ** formed the 2:1 complex with Al^{3+} and performed fluorescence quenching in MeCN/H_2O (95:5), which exhibited good selectivity and sensitivity. In addition, the mechanism of binding and fluorescence quenching was illustrated by titration experiment, Job' plot and DFT calculations.

Keywords: quinolinecarboxamide; Al^{3+} fluorescent sensor; coumarin; quenching mechanism

1.Introduction

Aluminum plays a significant role in our lives, such as pharmaceuticals, light alloys and water purification [1,2]. Emerging studies revealed that excessive intake of Al^{3+} ion in human body can cause Alzheimer's disease, amyotrophic lateral sclerosis, hemochromatosis, osteoporosis [3-5] etc., as well as environmental acidification increases the amount of free Al^{3+} ions [6]. Therefore, the development of specific fluorescent sensor for Al^{3+} detection is of great crucial in biological and environment research and a growing number of scientists are interested in the investigation of fluorescent sensors for Al^{3+} [7].

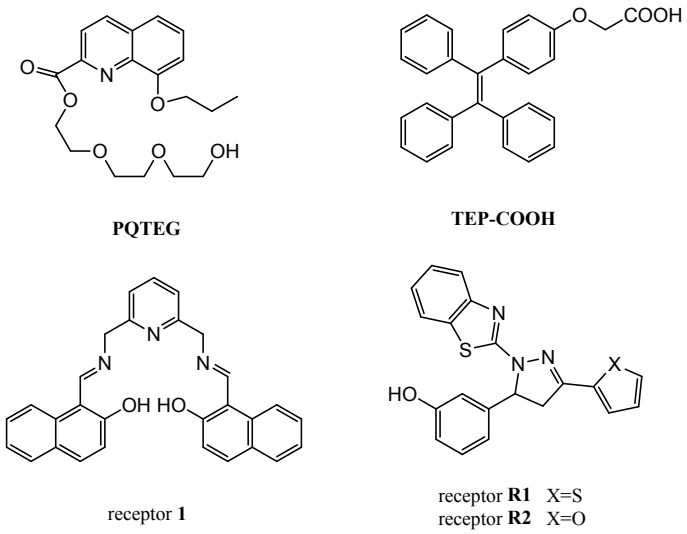

Scheme 1 Representative examples of Al^{3+} fluorescent sensor.

In past decades, a great number of fluorescent sensors have been designed in the detection of heavy metal ions for medical, biological and environmental science, which received great attention because of its advantages on simple, convenience and low cost [8-11]. The Al^{3+} chemosensors based on "turn on" type have been widely studied such as quinolone [12], hydrazinopyrimidine [13], Schiff base [14-16], etc. For example, as seen in Scheme 1, Jisha synthesized the quinoline derivative **PQTEG** as fluorescent probe acted as a visible colorimetric sensor for Al^{3+} [17]. Gui reported a novel tetraphenylethylene core **TEP-COOH** as "turn-on" chemosensor for Al^{3+} by using AIE effect and performed high selectivity toward Al^{3+} [18]. Schiff base is a familiar structure of Al^{3+} chemosensor, which can provide a hard-base environment to coordinate with the hard-acid Al^{3+} [19]. Lu designed a "turn-on" type Schiff-base **receptor 1** as fluorescent sensor for Al^{3+} in EtOH/H_2O (95:5 v/v) solution [20]. However, compared with the "turn-on" type, the "turn-off" type fluorescent sensor for Al^{3+} detection was rarely reported in literature, which usually has a lower detection limit [21]. Rangasamy designed thiophene and furan appended pyrazoline as fluorescent sensor receptors **R1** and **R2** for detection of Al^{3+} by using quenching mechanism [22]. Recently, coumarin derivatives are considered of the most attractive fluorophore groups with extensive research and application because of their high molar absorption coefficient, large Stokes shift, high fluorescence quantum yield, good physiological activity [23,24], which was suggested that coumarin could be used as desired fluorophore for the

designed of fluorescent chemosensor.

Herein, an effective "turn-off" type fluorescent sensor for Al^{3+} based on quinolinecarboxamide-coumarin molecule was designed and synthesized in this paper. The sensor **ZXQ** exhibited the blue fluorescence with high fluorescence quantum yield, which performed an excellent sensitive and selective response to Al^{3+}. Moreover, the DFT calculations were used to confirm the quenching mechanism.

2. Experimental

2.1. Materials and equipment

All of the chemicals used in the current study were purchased from commercial vendors and used as received without further purification, unless otherwise noted. All solvents were purified and dried using standard methods prior to use. The salts used in stock solutions of metal ions were $AgNO_3$, $Al(NO_3)_3$, $Co(NO_3)_2$, CuCl, $Cu(NO_3)_2$, $FeSO_4$, $Fe(NO_3)_3$, $HgCl_2$, $LiNO_3$, $MgSO_4$, $MnCl_2$, $NiCl_2$, $Pb(NO_3)_2$, $ZnCl_2$. Nuclear magnetic resonance (^1H, ^{13}C) spectra were recorded on a Bruker AM 500 spectrometer with chemical shifts reported as ppm at 500, 125 MHz, respectively, (in DMSO, $CDCl_3$ and TMS as the internal standard). The high-resolution mass spectra were recorded on a Thermo Scientific LTQ Orbitrap XL (ESI) and melting points (Mp.) were recorded on a X-4 electro-thermal digital melting point apparatus. All of the chemicals used in the current study were purchased from commercial vendors and used as received without further purification, unless otherwise noted. All solvents were purified and dried using standard methods prior to use.

2.2. Absorbance, fluorescence and quantum yield

UV-Vis absorption spectra were measured on a UV-2550. Fluorescence spectra were obtained with an Edinburgh FS5 spectrofluorometer. The solvents used in the photochemical measurements were spectroscopic grade. All the experiments were

performed repeatedly, and reproducible results were obtained. The Φ_F values in solution were measured using an integrating sphere method and dilute solutions of the compounds in organic solvent were used (1×10^{-5} mol/L). All the fluorescence spectra data were recorded 3 times.

2.3 General procedure for the synthesis of compounds

*2.3.1 General preparation of compounds 3-carboxycoumarin derivatives **2***

A mixture of salicylaldehyde **1a** (10.0 mmol, 1.210 g), meldrum's acid (10.0 mmol, 1.441 g) in ethanol (10 mL) was stirred to reflux for 12 h. The reaction was complete detected by TLC and cooled to room temperature, and then the reaction precipitate was filtered to give crude product. The crude product was purified by re-crystallized from anhydrous ethanol solvent (5 mL) to afford target compound **2a** (1.616 g, 85%) as white solid without further purification.

*2.3.2 General preparation of compounds 3-acyl chloride coumarin derivatives **3***

A mixture of 3-carboxycoumarin **2a** (10.0 mmol, 1.901 g), anhydrous thionyl chloride (4.0 mL) and anhydrous DMF (0.1 mL) was stirred at room temperature for 1 h. The reaction was complete detected by TLC and the solvent was removed under reduced pressure to afford target compound **3a** (1.447 g, 83%) as white solid.

*2.3.3 General preparation of compounds 3-carboxamide coumarin derivatives **HXQ** and **ZXQ***

3-Acyl chloride coumarin **3a** (0.4160 g, 2.0 mmol), Et_3N (2.021 g, 20.0 mmol), 2-quinolylamine (0.2884 g, 2.0 mmol) and $CHCl_3$ (10 mL) were added in turn to a 50 mL round-bottomed flask. The reaction was stirred for 12 h at room temperature and

completed the reaction was detected by TLC analysis. The mixture was washed with water (20 mL) and extracted with dichloromethane (3×25 mL). The organic layer was combinated and dried with Na_2SO_4, and then removed the solvent under reduced pressure. The residue was purified by silica gel chromatography eluting (silica gel, petroleum ether/ethyl acetate=4:1) to afford complex **HXQ** (0.08218 g, 26%) as an white solid.

*2.3.4 2-oxo-N-(quinolin-2-yl)-2H-chromene-3-carboxamide (compound **HXQ**)*

White solid. Yield 26%. Mp. 221-223 °C ^{1}H NMR (500 MHz, DMSO-d_6) δ(ppm): 11.41 (s, 1H), 9.10 (s, 1H), 8.47 (d, *J* = 10.6 Hz, 2H), 8.08 (d, *J* = 7.2 Hz, 1H), 7.96 (d, *J* = 8.0 Hz, 1H), 7.89 (d, *J* = 7.8 Hz, 1H), 7.85-7.81 (m, 1H), 7.74 (d, *J* = 7.8 Hz, 1H), 7.60 (t, *J* = 7.4 Hz, 1H), 7.55-7.47 (m, 2H). ^{13}C NMR (125 MHz, DMSO) δ(ppm): 165.93 (1C), 163.67 (1C), 154.18 (1C), 150.54 (1C), 146.47 (1C), 139.05 (1C), 134.88 (1C), 130.72 (1C), 130.40 (1C), 127.89 (1C), 127.39 (1C), 126.13 (1C), 125.52 (2C), 125.50 (1C), 124.33 (1C), 118.63 (1C), 116.39 (1C), 114.20 (1C). HRMS (ESI): m/z calcd for $C_{19}H_{12}N_2O_3^+$ $(M+Na)^+$ 339.0740, found 339.0745.

*2.3.5 7-(diethylamino)-2-oxo-N-(quinolin-2-yl)-2H-chromene-3-carboxamide (compound **ZXQ**)*

Yellow solid. Yield 46%. Mp. 317-318 °C. ^{1}H NMR (500 MHz, $CDCl_3$) δ(ppm): 11.52 (s, 1H), 8.81 (s, 1H), 8.56 (d, J = 8.9 Hz, 1H), 8.18 (d, J = 9.0 Hz, 1H), 7.95 (d, J = 8.4 Hz, 1H), 7.78 (d, J = 8.0 Hz, 1H), 7.66 (t, J = 7.7 Hz, 1H), 7.55-7.38 (m, 2H), 6.67 (dd, J = 8.9, 2.3 Hz, 1H), 6.55 (d, J = 2.2 Hz, 1H), 3.47 (q, J = 7.1 Hz, 4H), 1.26 (s, 6H). ^{13}C NMR (125 MHz, $CDCl_3$) δ(ppm): 162.52 (1C), 162.01 (1C), 158.09 (1C), 153.08 (1C), 151.29 (1C), 148.87 (1C), 139.94 (1C), 138.13 (1C), 131.49 (1C), 129.70 (1C), 128.06 (1C), 127.37 (1C), 126.39 (1C), 125.03 (1C), 115.09 (1C), 110.19 (1C), 109.83 (1C), 108.63 (1C), 96.77 (1C), 45.22 (2C), 12.46 (2C). HRMS (ESI): m/z calcd for $C_{23}H_{22}N_3O_3^+$ $(M+H)^+$ 388.16557, found 388.16525.

3. Results and discussion

3.1 Synthesis

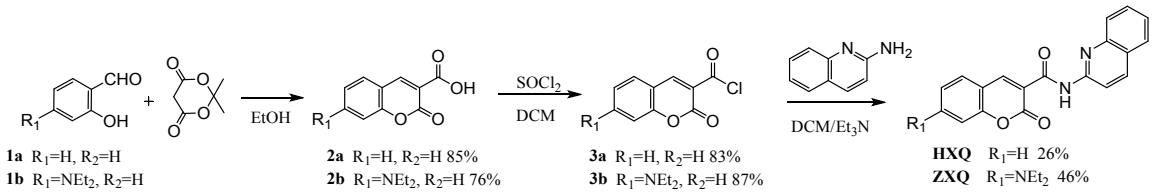

Scheme 2 Synthesis of **HXQ** and **ZXQ**.

Preparation route of target molecules **HXQ** and **ZXQ** were shown in scheme 2. Precursors 3-carboxycoumarin **2** were prepared by the reaction of salicylaldehyde derivatives with meldrum's acid in refluxing ethanol solution, which resulted in 85% (R_1 = H) and 76% (R_1 = NEt_2) yields. Then, with the acyl chloride reaction of thionyl chloride, the 3-carboxycoumarin **2** converted to 3-acyl chloride coumarin **3** in 83% (R_1 = H) and 87% (R_1 = NEt_2) yields. The target amide coumarin derivatives were produced by using the amide reaction of 3-acyl chloride coumarin **3** and 2-quinolylamine under Et_3N condition, which were yielded in 26% and 46%, respectively. The structures of **HXQ** and **ZXQ** were characterized by ^1H NMR, ^{13}C NMR and HR-MS analysis.

3.2 Fluorescence detection

*3.2.1 The solvent selection of **ZXQ***

The UV-Vis absorption and fluorescence emission spectra of **ZXQ** in different solvents were detected and shown in Fig. S1 (see in supporting information) and Table 1. **ZXQ** exhibited similar high sharp absorption peaks in different organic solvents, that its maximum absorption wavelength and the molar absorption coefficient (ε_{max}) were rarely affected by the solvent polarity. Meanwhile, the maximum absorption wavelength ranged in 428-440 nm, which displayed blue fluorescence and could be seen intuitively under 365 nm UV lamp (Fig. 1). The value of ε_{max} was approximately 7.0×10^4 $M^{-1}\cdot cm^{-1}$, except 5.2×10^4 $M^{-1}\cdot cm^{-1}$ in Toluene. Compared with the absorption spectra, the fluorescence emission spectra of **ZXQ** was much more affected by the solvent polarity. It is noteworthy that the fluorescence emission intensity of **ZXQ** was much stronger in non-polar solvent than in polar solvent. The fluorescence quantum yield (Φ_F) of **ZXQ** in DCM, $CHCl_3$, EA and THF were examined as 0.85, 0.88, 0.76

and 0.86, respectively, and its emission wavelength at around 460 nm. Moreover, the Φ_F of **ZXQ** was up to 0.92 in non-polar solvent toluene, with the emission wavelength at 449 nm.

Table 1 Optical data of **ZXQ** in solvents at room temperature.

Dye	Solvent	UV-Vis		Fluorescence		Stokes shift
		λ_{abs} (nm)[a]	ε_{max} ($M^{-1}\cdot cm^{-1}$)	λ_{em} (nm)	Φ_F[b]	(nm)
ZXQ	toluene	428	52100	449	0.92	21
	DCM	435	72200	466	0.85	31
	$CHCl_3$	434	73000	459	0.88	25
	EA	428	76700	463	0.76	32
	THF	429	74100	464	0.86	35
	MeCN	432	75500	475	0.15	43
	DMF	437	70900	481	0.07	44
	DMSO	440	68800	485	0.05	45
	EtOH	434	70300	477	0.09	43
	MeOH	434	64600	480	0.04	46

[a]All of the values correspond to the strongest absorption peaks.

[b]Fluorescence quantum yields (Φ_F) are measured using an integrating sphere method. Standard errors are less than 5%.

However, the fluorescence emission intensity significantly reduced and the emission peak underwent a slight red shift (10-30 nm) in polar solvents (MeCN, DMF, DMSO, EtOH, MeOH) compared with in non-polar solvents. The fluorescence quantum yield (Φ_F) of **ZXQ** was 0.15 in polar solvent MeCN with the emission wavelength at 475 nm. As well as the Φ_F of **ZXQ** reduced to less than 0.1 in strong polar solvents (DMF and DMSO) and proton solvents (EtOH and MeOH) with the emission wavelength at around 480 nm. Accordingly, the Stokes shift of **ZXQ** were ranged between 21 and 35 nm in toluene, DCM, $CHCl_3$, EA and THF. Whereas in polar solvents (MeCN, DMF, DMSO, EtOH, MeOH), **ZXQ** performed a slightly larger Stokes shift within 43-46 nm.

*3.2.2 Optical properties of **HXQ** and **ZXQ** in $CHCl_3$*

The UV-Vis absorption and fluorescence emission spectra of **HXQ** and **ZXQ** in

$CHCl_3$ were shown in Fig. 1. **HXQ** exhibited a broad absorption peak at about 310 nm in $CHCl_3$ and the value of ε_{max} was about 1.4×10^4 $M^{-1}\cdot cm^{-1}$. It can be seen that **HXQ** showed colorless in $CHCl_3$ under the visible light (Fig. 1 left, insert). However, the absorption intensity of **ZXQ** significantly enhanced and its maximum absorption wavelength (λ_{abs}) underwent an obvious red shift of 121 nm compared with **HXQ**. Accordingly, the λ_{abs} of the diethylamine substituted **ZXQ** at about 434 nm and the molar absorption coefficient (ε) was increased by approximately 5.2 times. Moreover, the introduction of diethylamino significantly enhanced the fluorescence emission intensity of **ZXQ**, while also caused a large red shift on emission wavelength. The emission wavelength of **ZXQ** (459 nm) was larger than **HXQ** (375 nm), suggesting that the substitution of diethylamine on the coumarin formed a push-pull structure which caused the molecular charge transfer (ICT). Meanwhile, the fluorescence quantum yield (Φ_F) was greatly increased from 0.03 (**HXQ**) to 0.88 (**ZXQ**). Thus, the Stokes shift of **HXQ** was 68 nm, yet **ZXQ** was decreased to 26 nm.

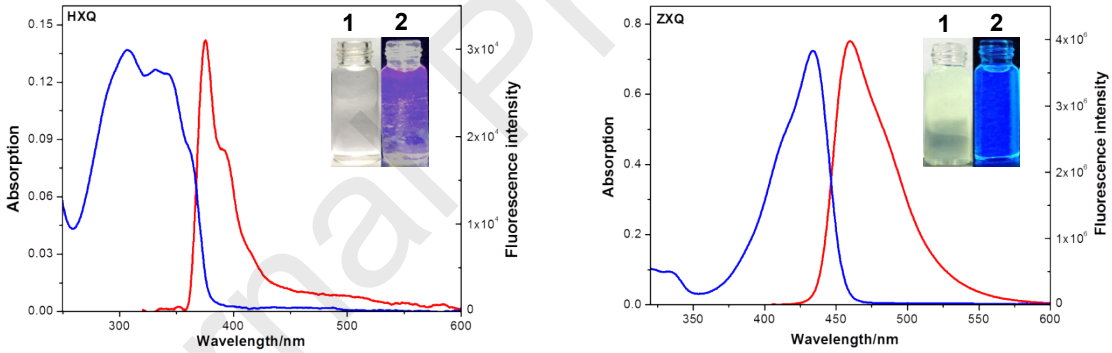

Fig. 1. UV-Vis absorption (blue) and fluorescence (red) spectra of **HXQ** (left) and **ZXQ** (right) in $CHCl_3$. Inset shows photographs of **HXQ** and **ZXQ** in $CHCl_3$ taken under (1) the visible light and (2) the 365 nm UV lamp.

3.2.3 Fluorescence spectral properties of detecting Al^{3+}

When studied the fluorescence properties of **HXQ** and **ZXQ**, we found that **ZXQ** can be quenched by Al^{3+}, so it can be used as the fluorescent probe for Al^{3+} detection. In order to determine the possibility of using **ZXQ** as the fluorescent probe for Al^{3+}, UV-Vis absorption and fluorescence emission spectra of **ZXQ** solution (1.0×10^{-5} mol/L) in MeCN/H_2O (95:5, v/v) before and after addition of Ag^+, Al^{3+}, Co^{2+}, Cu^+, Cu^{2+}, Fe^{2+}, Fe^{3+}, Hg^{2+}, Li^+, Mg^{2+}, Mn^{2+}, Ni^{2+}, Pb^{2+} and Zn^{2+} (1.0×10^{-5} mol/L) were measured and

shown in Fig. 2.

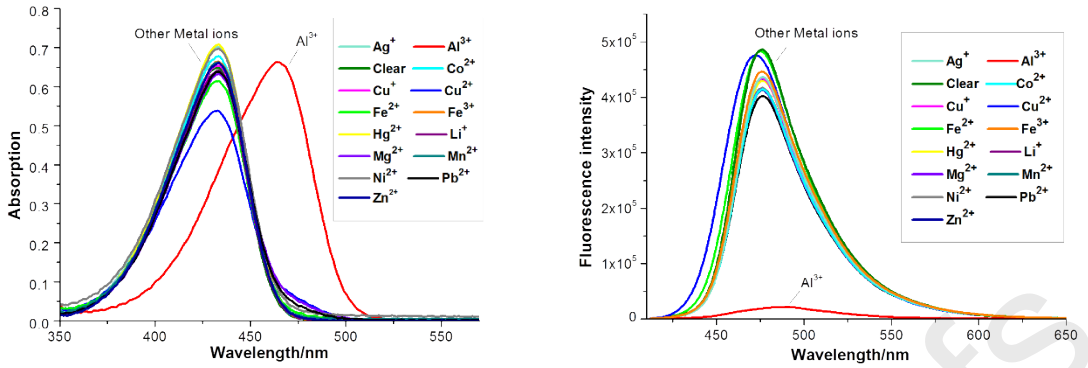

Fig. 2. Left: The absorption spectra of **ZXQ** (1.0×10^{-5} mol/L) in the presence of different metal ions in the MeCN/H_2O (95:5, v/v). Right: The Fluorescence spectra of **ZXQ** (1.0×10^{-5} mol/L) in the presence of different metal ions in the MeCN/H_2O (95:5, v/v).

The maximum absorption wavelength of **ZXQ** appeared an obvious red shift from 433 nm to 464 nm in the presence of Al^{3+}. However, the addition of other metal ions did not caused any obvious changes on the maximum absorption wavelength, while the molar absorption coefficient (ε) was increased in the presence of Hg^{2+}, Ag^{+}, Ni^{2+} and Co^{2+}, and decreased slightly after addition of Cu^{2+}, Fe^{2+}, Mg^{2+} and Pb^{2+}. Meanwhile, the color of **ZXQ** has been significantly deepened under the visible light after addition of Al^{3+} as shown in Fig. 3. More interestingly, the fluorescence of **ZXQ** was significantly quenched (see Fig. 2) and the emission wavelength underwent a red shift of 12 nm due to the presence of Al^{3+}. Nevertheless, the fluorescence emission spectra of **ZXQ** changed slightly with the presence of other metal ions. Accordingly, the emission wavelength of **ZXQ** underwent a slight blue shift of 5 nm in the addition of Cu^{2+} and the emission intensity became a little weaker. As well as the fluorescence intensity of **ZXQ** reduced a little after addition of other 12 metal ions. Furthermore, as shown in Fig. 3, **ZXQ** can be used to clearly distinguish Al^{3+} under 365 nm UV lamp and visible light. These interesting phenomenon indicated that **ZXQ** could be used as the "turn off" type fluorescent probe for detection Al^{3+}.

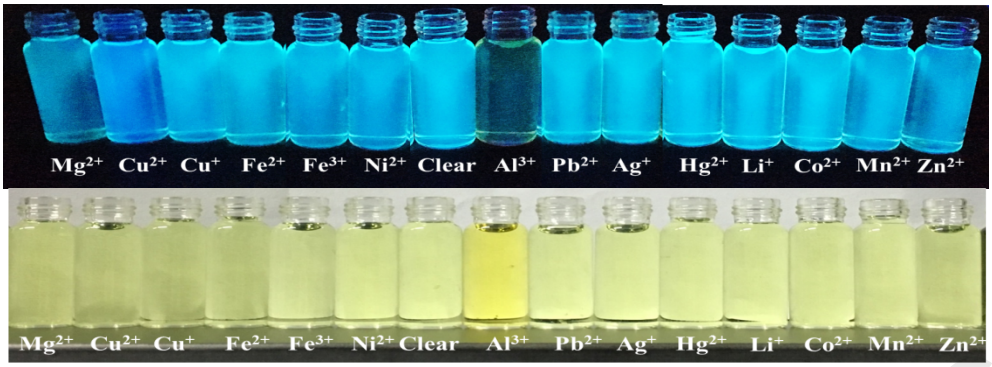

Fig. 3. The **ZXQ** under the 365 nm UV lamp (upper row) and the visible light (lower row) in the presence of different metal ions in the MeCN/H_2O (95:5, v/v) solution.

3. 3 Binding stoichiometry and sensing mechanism

To further understand the binding process of the fluorescent probe **ZXQ** for Al^{3+}, the chemical titration experiment based on fluorescence spectra analysis was performed. **ZXQ** (1.0×10^{-5} mol/L) with different concentrations of Al^{3+} (0.1×10^{-5}-1.0×10^{-5} mol/L) were prepared and their UV-Vis absorption spectra and fluorescence emission spectra were measured (see Fig. 4). It is observed that the absorption intensity of **ZXQ** decreased gradually with the concentration of Al^{3+} increased, whilst a new absorption peak appeared at about 464 nm. Additionally, when the concentration of Al^{3+} increased more than 0.5×10^{-5} mol/L, the absorption peak (433 nm) quickly disappeared with the intensity of new absorption peak (464 nm) increased (Fig. 4). It can be seen from Fig. 3 that as the concentrations of Al^{3+} gradually increased in the solutions of **ZXQ**, the fluorescence emission wavelength performmed a slight red shift, while the concentrations of Al^{3+} was increased to 0.5×10^{-5} mol/L, the maximum emission wavelengths were maintained at about 487 nm. Then, the fluorescence intensity of **ZXQ** rapidly decreased as the concentrations of Al^{3+} increased. The inset of Fig. 4 displayed the relationship between the Al^{3+} concentration and the maximum emission intensity of **ZXQ**+Al^{3+} solution. It is worth noting that the fluorescence was completely quenched with 0.5×10^{-5} mol/L Al^{3+}. When more Al^{3+} was titrated, the fluorescence intensity of **ZXQ** performed tiny change. Thus, the chemical titration experiment indicated that a 2:1 stoichiometry complex of **ZXQ** and Al^{3+} may be formed.

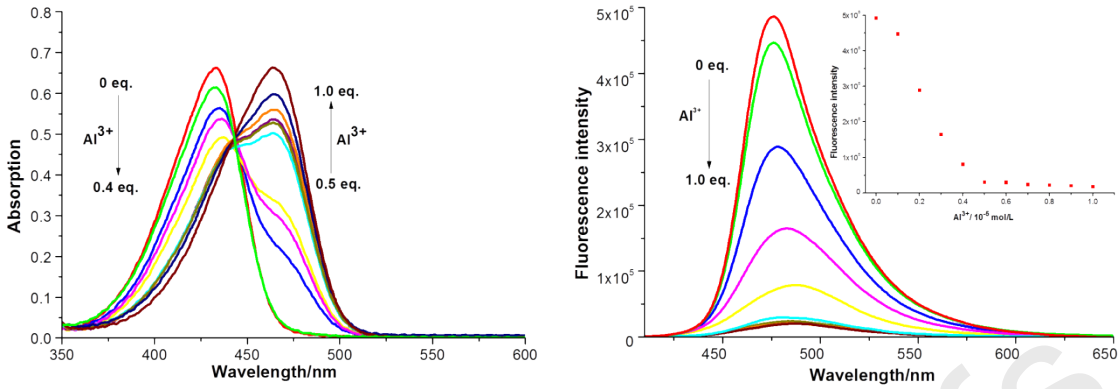

Fig. 4. UV-Vis absorption (left) and fluorescence (right) response of **ZXQ** (1.0×10^{-5} mol/L) exposed to Al^{3+} of various concentrations: 0.1×10^{-5}, 0.2×10^{-5}, 0.3×10^{-5}, 0.4×10^{-5}, 0.5×10^{-5}, 0.6×10^{-5}, 0.7×10^{-5}, 0.8×10^{-5}, 0.9×10^{-5}, 1.0×10^{-5} mol/L (from top to bottom). Inset shows fluorescence titration curve of **ZXQ** with Al^{3+}. These spectra were measured in MeCN/H_2O (95:5, v/v) solution.

In addition, Job's Plot based on fluorescence intensity was carried out (see Fig. 5). The total concentration of **ZXQ** and Al^{3+} was constant (1.0×10^{-5} mol/L) and the molar fraction of **ZXQ** ([ZXQ]/[ZXQ]+[Al^{3+}]) changed. As shown in Fig. 5, the result of Job's Plot displayed a maximum at 2/3 fraction **ZXQ** and it indicated that a 2:1 ligand-metal complex was formed between **ZXQ** and Al^{3+}. Therefore, it can be concluded that **ZXQ** and Al^{3+} formed a complex with a ratio of 2:1, which resulted in fluorescence quenched.

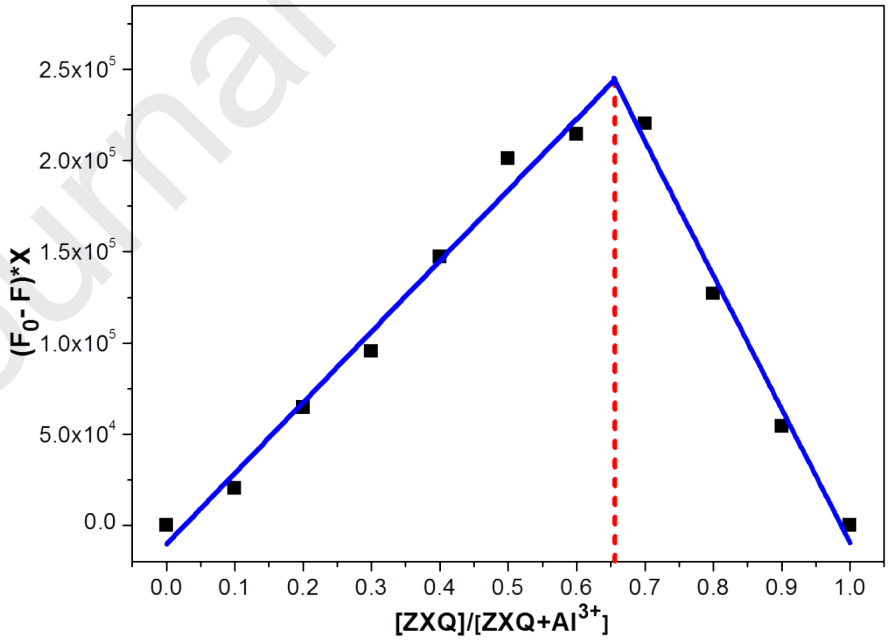

Fig. 5. Job's plot for determining the stoichiometry for **ZXQ** and Al^{3+} in MeCN/H_2O (95:5, v/v). Total concentration=1.0×10^{-5} mol/L.

Based on the above experimental analysis, the binding ratio of the probe **ZXQ** to Al^{3+} was verified to be 2:1. It can be seen from Scheme 3, an Al^{3+} coordinated with the oxygen atom of amide carbonyl and the nitrogen atom of quinoline on two **ZXQ** molecules.

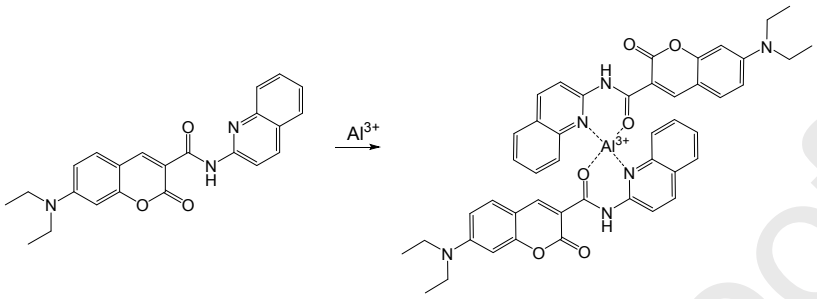

Scheme 3 The response mechanism of **ZXQ** to Al^{3+}.

To further investigate the sensing mechanism of **ZXQ** to Al^{3+}, a comparison was made on the ^1H NMR spectroscopy between the **ZXQ** and **ZXQ**+Al^{3+} (see Fig. S2 in supporting information). It can be seen from Fig. S2 that ^1H NMR spectroscopy of the complex **ZXQ**+Al^{3+} changed greatly compared to **ZXQ**. The chemical shift of NH single of the complex **ZXQ**+Al^{3+} has moved from 11.5 ppm to 12.7 ppm compared with **ZXQ** in $CDCl_3$. These observations indicated the ionization support our assumptions.

Meanwhile, we also investigated the interference of different metal ions on the recognition of Al^{3+} by fluorescent probe **ZXQ**. The fluorescence intensity of **ZXQ** at 487 nm was measured in the presence of different metal ions, including Ag^+, Al^{3+}, Co^{2+}, Cu^+, Cu^{2+}, Fe^{2+}, Fe^{3+}, Hg^{2+}, Li^+, Mg^{2+}, Mn^{2+}, Ni^{2+}, Pb^{2+} and Zn^{2+} (0.5×10^{-5} mol/L, respectively). When Al^{3+} (0.5×10^{-5} mol/L) was added into the solution of **ZXQ**+M, the blue bars exhibited the same fluorescence quenching effect (see Fig. 6). These studies clearly suggested that the probe **ZXQ** could be utilized for the selective detection of Al^{3+} without the interference from other metal ions.

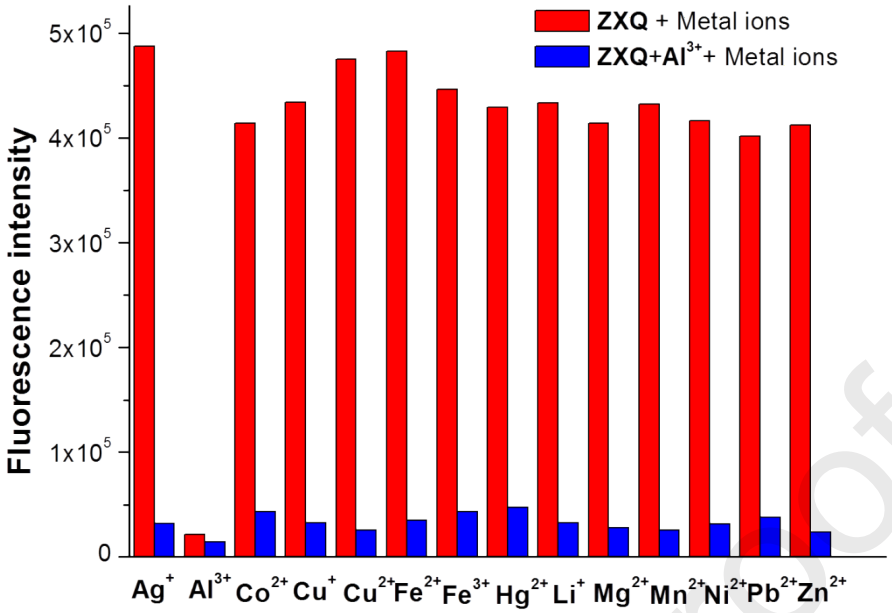

Fig. 6. Fluorescence intensities of **ZXQ** (1.0×10^{-5} mol/L) in the presence of various metal ions and Al^{3+} mixtures in MeCN/H_2O (95:5, v/v). The red bars represent the emission intensities of **ZXQ** in the presence of different metal ions, the blue bars represent the emission intensities of **ZXQ** in the presence of different metal ions and Al^{3+}.

3.4. Effect of pH on fluorescence properties

To investigate the effect of the fluorescence properties of **ZXQ** and **ZXQ**+Al^{3+} on the pH value, the UV-Vis absorption and fluorescence spectra of **ZXQ** and **ZXQ**+Al^{3+} (1.0×10^{-5} mol/L) in MeCN/H_2O (95:5, v/v) solution were measured at different pH values. The absorption spectra (Fig. 7) shown that the maximum absorption peak decreased and a new absorption peak appeared at 463 nm when the pH of the buffer solution decreased below 3. Meanwhile, **ZXQ** displayed a fluorescence quenching at approximately 478 nm when pH ≤ 3 and the fluorescence of **ZXQ** did not vary with pH over that range of 4 to 12 (Fig. 7). Moreover, with the addition of Al^{3+}, pH of buffer solution significantly affected the fluorescence intensity of **ZXQ**+Al^{3+} complex. When pH > 10, the fluorescence intensity of **ZXQ**+Al^{3+} complex displayed an enhancement at 478 nm, which was convenient for practical application of **ZXQ** to the determination of Al^{3+} at pH ranging from 4 to 10.

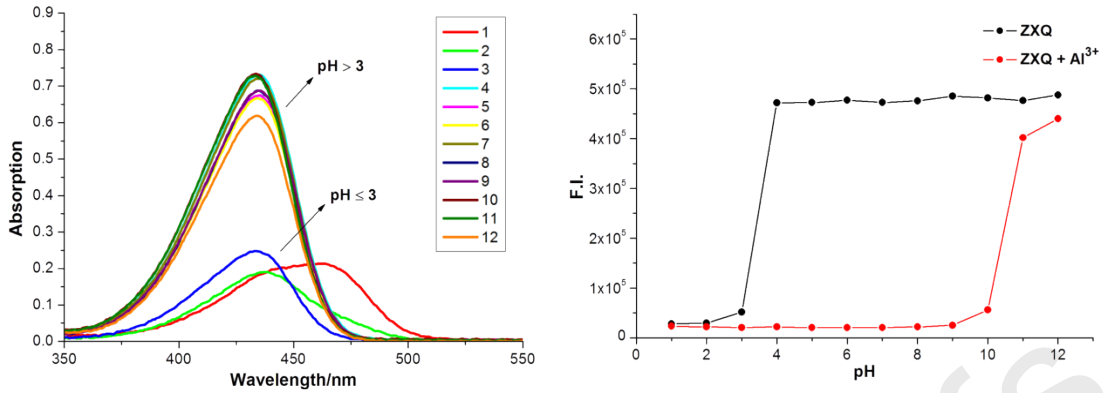

Fig. 7. Left: The absorption spectra of **ZXQ** (1.0×10^{-5} mol/L) with different pH in MeCN/H_2O (95:5, v/v). Right: effect of pH on the fluorescence intensity at 478 nm of **ZXQ** and **ZXQ**+Al^{3+} in MeCN/H_2O (95:5, v/v).

4. Theoretical calculation

4.1 Mechanism of detecting Al³

In order to further study the binding mechanism of Al^{3+} and probe **ZXQ**, density functional theory (DFT) calculations had been performed by applying the polarizable continuum model (PCM) at the B3LYP/6-311G(d) level in MeCN to optimize the structure of the fluorescent probe **ZXQ**, as implemented in the Gaussian 09 program package [25,26].

The stable structure and MEP surfaces of **ZXQ** were displayed in Fig. S3 (see in supporting information), the negative region represents with red color, while the positive region represents with blue color. Obviously, the negative region was concentrated between the oxygen atom of amide carbonyl and the nitrogen atom of quinoline, suggesting its potential to combine with Al^{3+} formed a stable six-membered ring.

According to the binding ratio of **ZXQ**: Al^{3+} acquired from the Job's plot experiment and the MEP simulation results, we proposed that one Al^{3+} coordinated with the oxygen atom of amide carbonyl and the nitrogen atom of quinoline on two **ZXQ** molecules. Fig. S4 (see in supporting information) displayed the geometry of metal-organic coordination clathrate **ZXQ**+Al^{3+} optimized using DFT calculation at the B3LYP/6-311G(d) level in MeCN, and the red region was the newly formed six-

membered ring. Further, we have calculated the Mülliken charge distribution about **ZXQ** and its metal complexes, and the results were shown in Table 2 and Fig. S4.

Table 2 Mülliken charge distribution of **ZXQ** and **ZXQ**+Al^{3+}.

	C (9-10)	C (21-24)	O (15)	NH (12,101)	O (7)	N (16)	O (13)	N (25)	Al (59)
ZXQ	-0.451	-0.371	-0.402	-0.315	-0.322	-0.382	-0.390	-0.376	
ZXQ+ Al^{3+}	-0.433	-0.047	-0.389	-0.281	-0.305	-0.361	-0.542	-0.798	1.423

It is clearly seen that the charge distribution of the coumarin ring and quinoline ring changed obviously, with the charge of the carbon atom (9-10) on the coumarin and the charge of the carbon atom (21-24) on the quinoline became more positive after binded with the Al^{3+}. Moreover, the charge of the oxygen atom (7, 14) and the nitrogen atom (12, 16) also became more positive in the formation of the complex, while the charge of the oxygen atom (13) and the nitrogen atom (25) become more negative, indicating that charge transfer had taken place. Meanwhile, the charge of Al^{3+} was 1.423, which was less than its apparent charge 3, suggesting that electron was transferred from **ZXQ** to Al^{3+}. As result, the positive charge of Al^{3+} delocalized to the electron cloud of the oxygen atom (13, 38) and the nitrogen atom (25, 50) to form a coordinate bond.

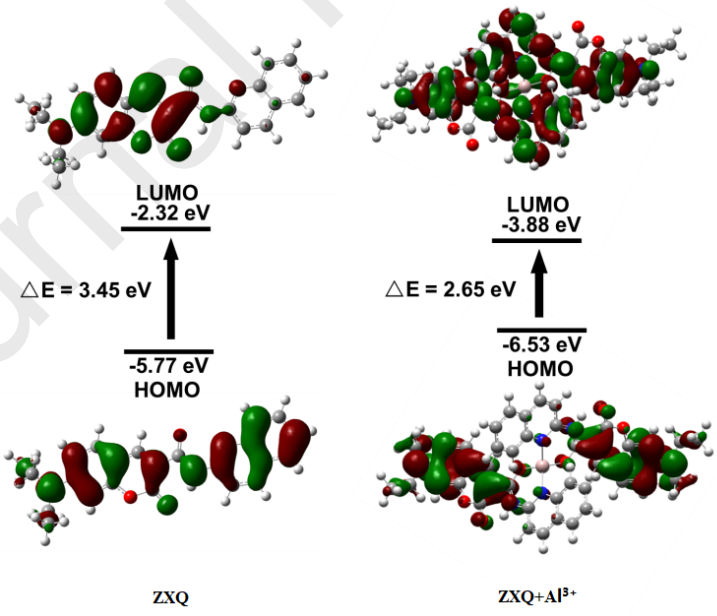

Fig. 8. Frontier molecular orbitals of **ZXQ** and metal-organic coordination clathrate **ZXQ**+Al^{3+}.

On the other hand, we also calculated the molecular frontier orbitals of probe **ZXQ** and the corresponding complex at the B3LYP/6-311G(d) level in MeCN. As shown in

Fig. 8, the HOMO of **ZXQ** was evenly distributed with a large conjugates and electron delocalization resulted an absorption wavelength red shift and an increase in fluorescence intensity. It is also apparent from the Fig. 8 that the HOMO of **ZXQ**+Al^{3+} complex was concentrated on the coumarin, while the LUMO was concentrated on the amide and quinoline. Therefore, it revealed that a strong intramolecular charge transfer (ICT) occurred, which lead to fluorescence quenching [27]. In addition, the energy gap of **ZXQ**+Al^{3+} complex was reduced to 2.65 eV lower than **ZXQ** (3.45 eV) lead to a red shift of the absorption and emission wavelength, which was consistent with the experimental results.

5. Conclusion

In summary, a "tun off" type Al^{3+} fluorescent probe **ZXQ** was designed and synthesized, which displayed blue fluorescence and high fluorescence quantum yield as well as favorable sensitivity and selectivity for the detection of Al^{3+}. The possible quenching mechanism of the Al^{3+} probe **ZXQ** was confirmed by chemometric methods and DFT calculations. From this, the probe **ZXQ** can be widely applied to biological, pharmaceutical and environmental monitoring.

Acknowledgement

We gratefully acknowledge the financial supported by the Natural Science Foundation of China (21606201) and the National Natural Science Foundation of Zhejiang (LY13B020016) and the Undergraduate Science and Technological Innovation Program in Zhejiang Province (Zhejiang Xinmiao Talents Program) (2017R403066).

References

[1] C.S. Cronan, W.J. Walker, P.R. Bloom, Predicting aqueous aluminium concentrations in natural waters, Nature 324 (1986) 140-143. doi:10.1038/324140a0.

[2] D.T. Quang, J.S. Kim, Fluoro- and Chromogenic Chemodosimeters for Heavy

Metal Ion Detection in Solution and Biospecimens, Chem. Rev. 110 (2010) 6280-6301. doi: 10.1021/cr100154p.

[3] S.C. Bondy, Low levels of aluminum can lead to behavioral and morphological changes associated with Alzheimer's disease and age-related neurodegeneration, Neurotoxicology 52 (2016) 222-229. doi:10.1016/j.neuro.2015.12.002.

[4] D.P. Perl, D.C. Gajdusek, R.M. Garruto, R.T. Yanagihara, C.J. Gibbs, Intra neuronal aluminium accumulation in amyotrophic lateral sclerosis and Parkinsonism-dementia of Guam, Science 217 (1982) 1053-1055. doi:10.1126/science.7112111.

[5] S.C. Bondy, The neurotoxicity of environmental aluminium is still an issue. Neurotoxicology 31 (2010) 575-581. doi:10.1016/j.neuro.2010.05.009.

[6] A. Becaria, A. Campbell, S.C. Bondy, Aluminum as a toxicant - eScholarship, Toxicol. Ind. Health 18 (2002) 309-320. doi:10.1191/0748233702th157oa.

[7] C.X. Wang, B. Wu, W. Zhou, Q. Wang, H. Yu, K. Deng, J.M. Li, R.X. Zhuo, S.W. Huang, Turn-on fluorescent probe-encapsulated micelle as colloidally stable nanochemosensor for highly selective detection of Al^{3+} in aqueous solution and living cell imaging, Sens. Actuators B Chem. 271 (2018) 225-238. doi:10.1016/j.snb.2018.05.079.

[8] J. Zheng, F. Huang, Y.J. Li, Q. Ye, J.H. Jia, L. Han, J.R. Gao, A highly selective copper fluorescent indicator based on a boron complex, J. Chem. Res. 39 (2015) 36-40. doi:10.3184/174751914X14190791988509.

[9] H.Q. Li, X.Q. Sun, T. Zheng, Z.X. Xu, Y.X. Song, X.H. Gu, Coumarin-based multifunctional chemosensor for arginine/lysine and Cu^{2+}/Al^{3+} ions and its Cu^{2+} complex as colorimetric and fluorescent sensor for biothiols, Sens. Actuators B Chem. 279 (2019) 400-409. doi:10.1016/j.snb.2018.10.017.

[10] C.J. Hua, H. Zheng, K. Zhang, M. Xin, J.R. Gao, Y.J. Li, A novel turn off fluorescent sensor for Fe(III) and pH environment based on coumarin derivatives: the fluorescence characteristics and theoretical study, Tetrahedron 72 (2016) 8365-8372. doi: 10.1016/j.tet.2016.08.023.

[11] B. Sen, S.K. Sheet, R. Thounaojam, R. Jamatia, A.K. Pal, K. Aguan, S. Khatua, A coumarin based Schiff base probe for selective fluorescence detection of Al^{3+} and

its application in live cell imaging, Spectrochim. Acta A 173 (2017) 537-543. doi: 10.1016/j.saa.2016.10.005.

[12] S.B. Roy, K.K. Rajak, A quinoline appended naphthalene derivative based AIE active turn-on fluorescent probe for the selective recognition of Al^{3+} and colourimetric sensor for Cu^{2+}: experimental and computational studies, J. Photochem. Photobiol. A 332 (2017) 505-514. doi: 10.1016/j.jphotochem.2016.09.015.

[13] B. Das, S. Dey, G. P. Maiti, A. Bhattacharjee, A. Dhara, A. Jana, Hydrazinopyrimidine derived novel Al^{3+} chemosensor: molecular logic gate and biological applications, New J. Chem. 42 (2018) 9424-9435. doi:10.1039/C7NJ05095J.

[14] H.Y. Liu, T.Q. Liu, J. Li, Y.M. Zhang, J.H. Li, J. Song, J.L. Qu, W.Y. Wong, A simple Schiff base as dual-responsive fluorescent sensor for bioimaging recognition of Zn^{2+} and Al^{3+} in living cells, J. Mater. Chem. B 6 (2018) 5435-5442. doi:10.1039/C8TB01743C.

[15] R. Singh, S. Samanta, P. Mullick, A. Ramesh, G. Das, Al^{3+} sensing through different turn-on emission signals vis-a-vis two different excitations: applications in biological and environmental realms, Analytica Chimica Acta 1025 (2018) 172-180. doi:10.1016/j.aca.2018.03.053.

[16] D. Singhal, N. Gupta, A.K. Singh, Fluorescent sensor for Al^{3+} ion in partially aqueous media using julolidine based probe, New J. Chem. 40 (2016) 7536-7541. doi:10.1039/C6NJ00348F.

[17] B. Jisha, M.R. Resmi, R.J. Maya, R.L. Varma, Colorimetric detection of Al(III) ions based on triethylene glycol appended 8-propyloxy quinoline ester, Tetrahedron Lett. 54 (2013) 4232-4236. doi:10.1016/j.tetlet.2013.05.134.

[18] S.L. Gui, Y.Y. Huang, F. Hu, Y.L. Jin, G.X. Zhang, L.S. Yan, D.Q. Zhang, R. Zhao, Fluorescence turn-on chemosensor for highly selective and sensitive detection and bioimaging of Al^{3+} in living cells based on ion-induced aggregation, Anal. Chem. 87 (2015) 1470-1474. doi:10.1021/ac504153c.

[19] S. Zeng, S.J. Li, X.J. Sun, M.Q. Li, Z.Y. Xing, J.L. Li, A benzothiazole-based

chemosensor for signifcant fluorescent turn-on and ratiometric detection of Al^{3+} and its application in cell imaging, Inorganica Chimica Acta 486 (2019) 654-662. doi:10.1016/j.ica.2018.11.042.

[20] C.Y. Lu, Y.W. Liu, P.J. Hung, C.F. Wan, A.T. Wu, A turn-on and reversible Schiff-base fluorescence sensor for Al^{3+} ion, Inorg. Chem. Commun. 35 (2013) 273-275. doi:10.1016/j.inoche.2013.06.005.

[21] Y.P. Li, X.H. Zhu, S.N. Li, Y.C. Jiang, M.C. Hu, Q.G. Zhai, Highly selective and sensitive turn-off−on fluorescent probes for sensing Al^{3+} ions designed by regulating the excited-state intramolecular proton transfer process in metal-organic frameworks, ACS Appl. Mater. Interfaces 11 (2019) 11338-11348. doi: 10.1021/acsami.8b20410

[22] M. Rangasamy, K. Palaninathan, Thiophene and furan appended pyrazoline based fluorescent chemosensors for detection of Al^{3+} ion, Inorg. Chem. Commun. 101 (2019) 177-183. doi:10.1016/j.inoche.2019.01.038.

[23] S. Goswami, A.K. Das, S. Maity, 'PET' vs. 'push-pull' induced ICT: a remarkable coumarinyl-appended pyrimidine based naked eye colorimetric and fluorimetric sensor for the detection of Hg^{2+} ions in aqueous media with test trips, Dalton Trans. 42 (2013) 16259-16263. doi:10.1039/C3DT52252K.

[24] Z. C. Zhou, A. N. Zheng, Y. H. Cui, Z. Q. Lin, W. J. Niu, Y. J. Zhang, J. R. Gao, Y. J. Li, Rational design and synthesis of 3-heteroaromatics coumarin molecules with unusual solution and solid dual efficient luminescence. Tetrahedron 75 (2019) 2958-2964. doi: doi.org/10.1016/j.tet.2019.04.034.

[25] M.J. Frisch, G.W. Trucks, H.B. Schlegel, G.E. Scuseria, M.A. Robb, J.R. Cheeseman, V.G. Zakrzewski, J.A. Montgomery, R.E. Stratmann, J.C. Burant, S. Dapprich, J.M. Millam, A.D. Daniels, K.N. Kudin, M.C. Strain, O. Farkas, J. Tomasi, V. Barone, M. Cossi, R. Cammi, B. Mennucci, C. Pomelli, C. Adamo, S. Clifford, J. Ochterski, G. A. Petersson, P.Y. Ayala, Q. Cui, K. Morokuma, D.K. Malick, A.D. Rabuck, K. Raghavachari, J.B. Foresman, J. Cioslowski, J.V. Ortiz, B.B. Stefanov, G. Liu, A. Liashenko, P. Piskorz, I. Komaromi, R. Gomperts, R.L. Martin, D.J. Fox, T. Keith, M.A. Al-Laham, C.Y. Peng, A. Nanayakkara, C.

Gonzalez, M. Challacombe, P.M.W. Gill, B.G. Johnson, W. Chen, M.W. Wong, J.L. Andres, M. Head-Gordon, E.S. Replogle, J.A. Pople, Gaussian 09; Gaussian: Wallingford, CT, 2009.

[26] E.J. Borkowski, F.M. Cecati, F.D. Suvire, D.M. Ruiz, C.E. Ardanaz, G.P. Romanelli, R.D. Enriz, Mass spectrometry and theoretical calculations about the loss of methyl radical from methoxilated coumarin, J. Mol. Struct. 1093 (2015) 49-58. doi:10.1016/j.molstruc.2015.03.007.

[27] Sheik Dawood Shahida Parveena, Basuvaraj Suresh Kumar a, Sekar Raj Kumar a, Raihana Imran Khana, Kasi Pitchumani. Isolation of biochanin A, an isoflavone, and its selective sensing ofcopper(II) ion, Sens. Actuators B Chem. 221 (2015) 75-80. doi:10.1016/j.snb.2015.06.060.

Zichun Zhou:
Graduated from Zhejiang University of Technology with a master's degree. The main research direction is the synthesis of organic dye molecules.

Wenjie Niu:
Graduated from Zhejiang University of Technology with a master's degree. The main research direction is the synthesis of organic dye molecules.

Zhangqi Lin:
Graduated from Zhejiang University of Technology with a master's degree. The main research direction is the synthesis of organic dye molecules.

Yanhong Cui:
Associate Professor, Zhejiang University of Technology, PhD, research direction is computational chemistry.

Yujin Li:
Associate Professor, Zhejiang University of Technology, PhD, research direction is green organic synthesis.

Wenjie Niu

Zhangqi Lin

Xue Tang

Yanhong Cui

Conflict of interest

We declare that we have no financial and personal relationships with other people or organizations that can inappropriately influence our work, there is no professional or other personal interest of any nature or kind in any product, service and/or company that could be construed as influencing the position presented in, or the review of, the manuscript entitled.

Graphic abstract

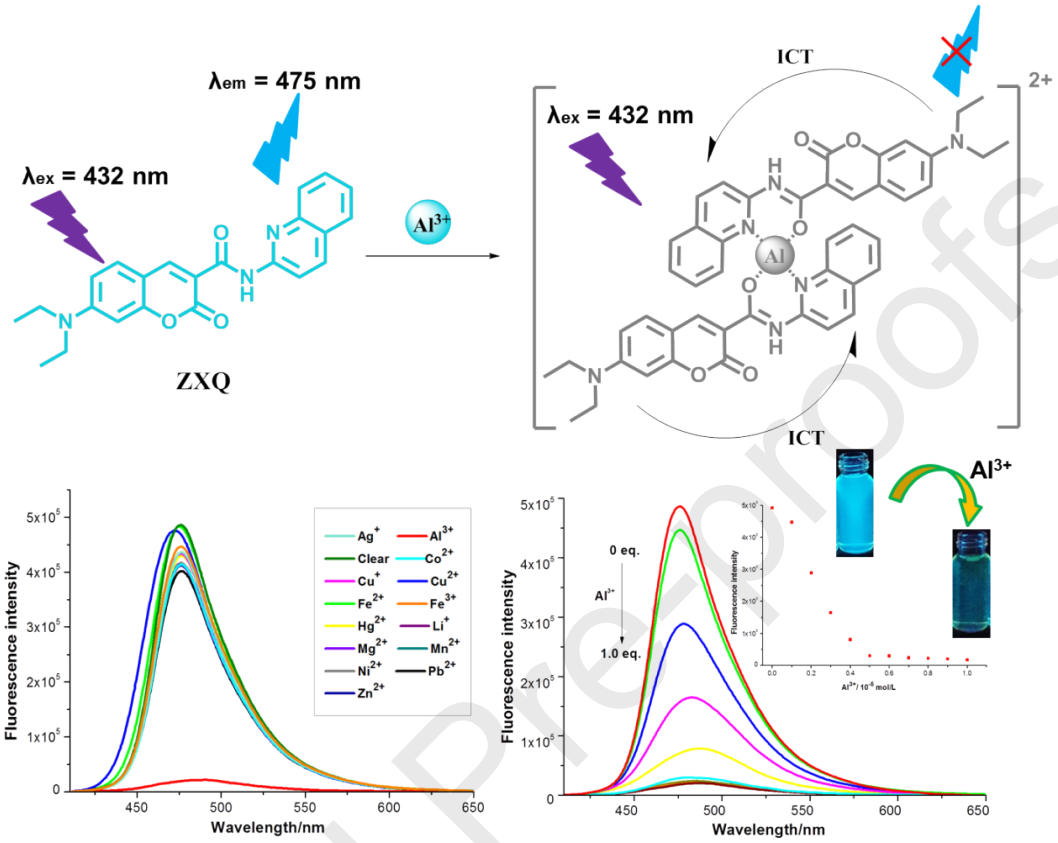

Highlights

- Quinolinecarboxamides based on coumarin derivatives were efficiently designed and synthesized.
- Probe **ZXQ** formed the 2:1 complex with Al^{3+} and performed fluorescence quenching, which showed good selectivity and sensitivity.
- The mechanism of binding and fluorescence quenching was illustrated by titration experiment, Job' plot and DFT calculations.